THE JOURNAL OF PHYSICAL CHEMISTRY A

ARTICLE

pubs.acs.org/JPCA

# Interfacial Chemistry of Poly(methyl methacrylate) Arising from Exposure to Vacuum-Ultraviolet Light and Atomic Oxygen

Hanqiu Yuan, Daniel R. Killelea, Sanja Tepavcevic,[†] Scott I. Kelber,[‡] and S. J. Sibener*

The James Franck Institute and Department of Chemistry, Gordon Center for Integrative Science, The University of Chicago, 929 E. 57th Street, Chicago, Illinois 60637, United States

**ABSTRACT:** We herein report on the chemical and physical changes that occur in thin films of poly(methyl methacrylate), PMMA, induced by exposure to high-energy vacuum ultraviolet radiation and a supersonic beam of neutral, ground electronic state O($^3$P) atomic oxygen. A combination of in situ quartz crystal microbalance and in situ Fourier-transform infrared reflection−absorption spectroscopy were used to determine the photochemical reaction kinetics and mechanisms during irradiation. The surface morphological changes were measured with atomic force microscopy. The results showed there was no enhancement in the mass loss rate during simultaneous exposure of vacuum ultraviolet (VUV) radiation and atomic oxygen. Rather, the rate of mass loss was impeded when the polymer film was exposed to both reagents. This study elucidates the kinetics of photochemical and oxidative reaction for PMMA, and shows that the synergistic effect involving VUV irradiation and exposure to ground state atomic oxygen depends substantially on the relative fluxes of these reagents.

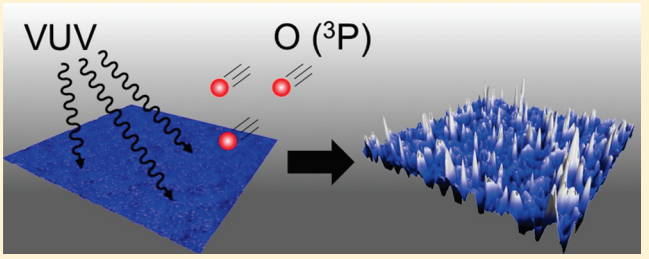


## 1. INTRODUCTION

Photochemical and oxidative reactions taking place at the vacuum−polymer interface are of technological significance for a wide variety of material and surface treatment processes including applications in spacecraft engineering.[1−3] Although the reactions caused by exposure of polymeric materials to ultraviolet (UV) radiation and oxygen are virtually ubiquitous, the understanding of how photo-oxidation proceeds in the presence of energetic oxidants remains unsettled.[1,4−6] For plasma processing techniques to realize their ultimate utility, a thorough understanding of the kinetics and dynamics of UV photochemistry and oxidation of polymers is necessary. Oxygen and UV radiation are widely employed for microlithography of polymers,[7] precise photoresist etching,[8] and the modification of wettability, adhesion, and other surface properties of polymer materials[5,9] and biomaterials.[10] Moreover, spacecraft are exposed to both vacuum ultraviolet (VUV) radiation and atomic oxygen in low Earth orbit (LEO). The possibility that the presence of both atomic oxygen and VUV light synergistically modify surface reactions is of particular significance.

Here, reactions involving ultrathin poly(methyl methacrylate), PMMA, films and VUV ($\lambda \leq 200$ nm) light and gas-phase atomic oxygen were investigated to elucidate fundamental photochemical and oxidative mechanisms. PMMA has multiple photochemical reaction pathways (Figure 1) and is reactive toward atomic oxygen, resulting in a rich system where many reactive channels may contribute to the observed reactivity, and determination of the dominant channels under given conditions is challenging. In addition, studies of the surface morphological changes due to VUV exposure highlight the importance of the vacuum−polymer interface.

Depending on the wavelength of the UV light, there are several possible photochemical reactions that may take place in PMMA (Figure 1).[11,12] Theoretical models[13,14] and experimental observations[1,2,15−17] have established the reaction to be a largely photochemical (as opposed to thermal) process where radicals are generated from UV-induced bond rupture. So far, most photochemical studies of PMMA used 200−300 nm UV radiation and found that the primary photoreaction mechanism was either whole or partial group ester side chain photolysis (Norrish type I, mechanism 3 in Figure 1). However, for VUV light, the more energetic photons could potentially rupture any bond in the PMMA repeating unit. UV/VUV laser ablation studies have not clearly identified a primary photoreaction pathway. Separate studies have pointed to either main chain scission yielding the MMA monomer[15] or partial ester group dissociation[18] as the dominant photoreactions for PMMA. A recent simulation[14] of VUV laser ablation of PMMA predicted that main-chain scission would be a minority channel and that side-chain ester photolysis would still be the dominant channel over a range of laser intensities. Another report[19] suggested that, despite the difference in photon energy for 193 and 248 nm lasers, the same photochemical processes took place. In the present study, thin PMMA films were exposed to a broadband VUV light source to determine the dominant mechanism of VUV photochemistry.

Atomic oxygen reacts with many polymeric materials,[2,6] and there are still unresolved issues regarding the fundamental reaction mechanisms and dynamics. In the present study, ultrathin films of PMMA were exposed to a supersonic beam of

**Special Issue:** Graham R. Fleming Festschrift

**Received:** July 2, 2010
**Revised:** July 30, 2010
**Published:** August 19, 2010

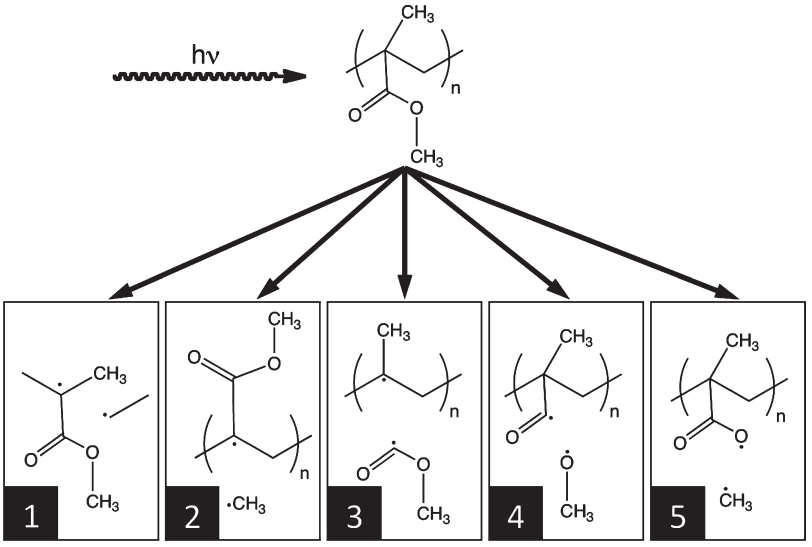


**Figure 1.** Possible PMMA ultraviolet photochemical reaction mechanisms. Shown are five possible mechanisms for VUV photodissociation of PMMA. Mechanism 3 is Norrish type I ester side-chain photolysis.

atomic oxygen (AO) in order to elucidate the role of atomic oxygen in surface reactions in the absence of ions or ultraviolet light from plasma.

A key question that has emerged from the studies of UV and AO reactions with polymers is under what conditions atomic oxygen and VUV may act synergistically to change the reaction rate. The reagents would be considered to act synergistically when the reaction rate during combined exposures differs from the sum of the rates measured during exposures to either reagent alone. Either there may be positive synergy, where the rate is accelerated, or negative, where the rate is inhibited. An electronic structure calculation[13] of the reaction of UV and AO with PMMA predicted that the addition of oxygen atoms would accelerate UV-induced mass loss by forming stable molecules through exothermic reactions. Different results have been observed for various polymeric systems under different experimental conditions. Co-exposure of polymers to VUV and AO enhanced the reaction rate for polyethylene,[12,20,21] fluoropolymers,[1,6,10,20,22] and polyimides,[23] but no enhancement was found for polypropylene,[9] polyolefins,[24] or PMMA;[2] and one report[1] found a decrease in mass loss during coexposure. The observed reaction rates must be studied as functions of the relative fluxes of each reagent, to determine the kinetics of these processes.

The goals of the present study were to elucidate the most significant VUV photochemical pathway, determine the kinetics of VUV and AO reactions, and investigate how the combination of AO and VUV alter the reaction rate for ultrathin films of PMMA. A quartz-crystal microbalance (QCM) was employed to directly measure mass changes in the films and Fourier-transform infrared reflection−absorption spectroscopy (IRRAS) was used to determine the chemical changes during VUV exposure. The surface morphological changes from VUV exposure were measured with atomic force microscopy (AFM).

## 2. EXPERIMENTAL SECTION

PMMA thin-film samples were prepared by spin-coating 2 wt % PMMA (FW = 9.50 kg mol$^{-1}$, Aldrich) in chlorobenzene on a 10 mm × 10 mm polycrystalline Au−mica substrate (atomically flat, Agilent) for IRRAS measurements or on a circular 14 mm diameter AT cut gold crystal sensor (Cr adhesive layer, intrinsic frequency 6 MHz, Maxtek Inc.) for the QCM measurements. The PMMA film was then annealed at 450 K for 1 h in air. The film thickness was determined to be 110 ± 10 nm by AFM and ellipsometry. This thickness was significantly thinner than the penetration depth of VUV radiation, which is 150 nm for 157 nm light[25] and is 192 nm for 160 nm light.[26] The VUV light is therefore interacting with the entire sample, not just the outermost layer.

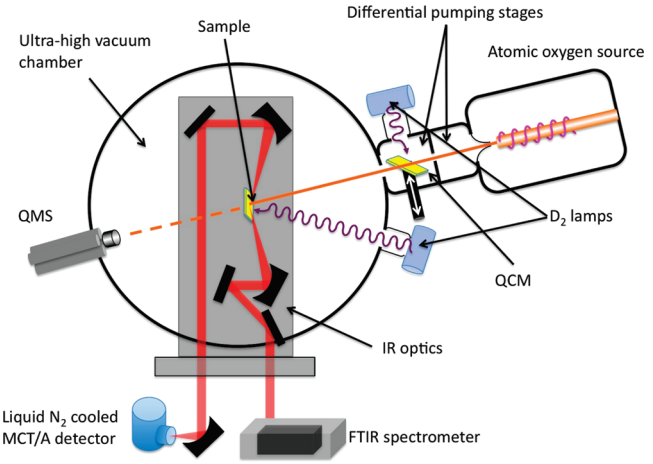


**Figure 2.** Schematic of experimental apparatus. The PMMA sample may be mounted on either a precision manipulator housed in a UHV chamber for FTIR measurements or in the second stage of differential pumping for QCM measurements.

In situ experiments were conducted in a molecular beam scattering apparatus (Figure 2), which consisted of an ultrahigh vacuum (UHV) surface-scattering chamber coupled to a supersonic molecular beamline. A more detailed description has been provided previously,[27−29] so only a brief description including the recent modifications are included here. A broad band $D_2$ lamp (Hamamatsu L7293, $MgF_2$ window) generated VUV radiation (112−400 nm, peak output near 160 nm[30]). The lamp


dx.doi.org/10.1021/jp1061368 |J. Phys. Chem. A 2011, 115, 3736–3745

was mounted 30 cm from the sample and 15° from the surface normal; the output power at this distance was 350 $\mu$W cm$^{-2}$. A FT-IR spectrometer (Nicolet 6700) was coupled to the UHV chamber to perform in situ IRRAS measurements. The p-polarized IR beam was focused on the sample at an incident angle of 75° with p-polarization and then directed onto the active element of a liquid-nitrogen-cooled mercury cadmium telluride (MCT/A) detector. The detector and the optics outside the UHV chamber were mounted in a dry-$N_2$ purged chamber. The IRRAS spectra were collected with a resolution of 4 cm$^{-1}$ and were averaged over at least 25 scans.

The supersonic molecular beamline (Figure 2) consisted of a beam source chamber and two stages of differential pumping. The first differential stage housed a chopper wheel for time-of-flight (TOF) measurements and a flag for blocking the beam. The QCM was mounted on a vertical manipulator in the second differential pumping stage for exposure to the atomic oxygen beam, which was centered on the QCM. This stage was also equipped with a second $D_2$ lamp, perpendicular to the beam axis, which could be positioned at four different distances from the sample to modulate the intensity of the light. The light intensity was measured to be 790 $\mu$W cm$^{-2}$ at 20 cm, 350 $\mu$W cm$^{-2}$ at 30 cm, 220 $\mu$W cm$^{-2}$ at 38 cm, and 120 $\mu$W cm$^{-2}$ at 51 cm. The photon flux ($\Phi_{VUV}$) was calculated to be $6.3 \times 10^{14}$, $2.8 \times 10^{14}$, $1.8 \times 10^{14}$, and $9.8 \times 10^{13}$ h$\nu$ cm$^{-2}$ s$^{-1}$, for the above intensities, by treating the light as monochromatic radiation with $\lambda$ = 160 nm. The sample was positioned at normal incidence to the atomic oxygen beam for AO-only exposure or facing the $D_2$ lamp for VUV-only exposure. For combined VUV/AO exposures, the sample was oriented 45° with respect to both the atomic beam and the $D_2$ lamp (20 cm from the sample). The uncertainty of the QCM measurements was found to be insignificant, less than $1 \times 10^{-5}$ $\mu$g s$^{-1}$ cm$^{-2}$.

A radio frequency plasma source[27] was used to generate a supersonic atomic oxygen beam formed by expanding 5% $O_2$ in Ne (60 Torr stagnation pressure) through a custom designed water-cooled quartz nozzle. The beam impinged on a 3 mm circular beam spot on the sample surface. The oxygen dissociation rate was 50%, which resulted in a flux ($\Phi_{AO}$) of $2.0 \times 10^{14}$ O atoms s$^{-1}$ cm$^{-2}$ with an average kinetic energy ($E_{trans}$) of 25 kJ mol$^{-1}$. Oxygen flux could be halved by moving a 50% duty cycle chopper wheel into the beam path. Any residual ionic species were deflected out of the beam by passing the beam through a deflector plate biased at 1.5 kV, although there was no evidence of ions in the TOF characterization of the beam.[27] The contribution of metastable electronically excited Ne atoms or UV light from the plasma source to the observed reactivity was checked by separate exposures to a beam generated by a 100% Ne plasma. The mass loss rate was significantly lower than the observed atomic oxygen mass loss rates. This background reactivity was then subtracted from the atomic oxygen data to account for the small mass loss due to non-atomic oxygen mass-loss channels.

The VUV irradiated PMMA films were imaged in contact mode by a Veeco Multimode IV AFM with silicon nitride tips under ambient conditions. The AFM imaged a 10 $\mu$m × 10 $\mu$m area (256 × 256 pixels), and images were taken from several regions of each sample. The images shown here are representative of the images collected.

## 3. RESULTS AND DISCUSSION

A combination of QCM and IRRAS experiments showed that VUV irradiation of PMMA thin films induced mass loss that followed first order kinetics with respect to both VUV flux and the PMMA film thickness. The dominant reaction mechanism was found to be Norrish type I ester side group photolysis that liberated methyl formate from the polymer. AFM measurements showed surface roughening as VUV exposure proceeded. Mass loss due to oxygen beam exposure followed first order kinetics with respect to oxygen flux and zeroth order with respect to the PMMA film thickness, consistent with surface reaction of the oxidant. Oxygen bombardment was largely a surface phenomenon whereas VUV irradiation penetrated the entire film. A synergistic deceleration of mass loss was observed in the regime where mass loss rate caused by either VUV or oxygen atoms was nearly the same.

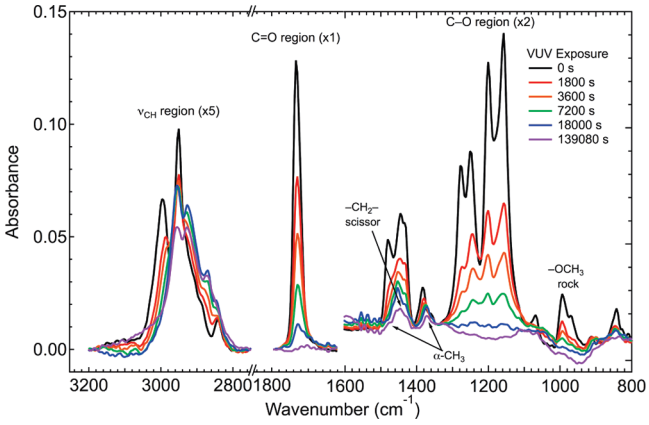


**Figure 3.** IRRAS spectra for VUV irradiation of PMMA. IRRAS spectra taken after various exposures to VUV ($\Phi_{VUV}$ = 350 $\mu$W, 2.82 × $10^{14}$ h$\nu$ cm$^{-2}$ s$^{-1}$). The IR absorption spectra from 3200 to 800 cm$^{-1}$ are shown. The $\nu_{CH}$ region (2800−3200 cm$^{-1}$) is magnified by a factor of 5, the C═O stretch (1600−1800 cm$^{-1}$) is unscaled, and the final portion, the carbonyl region (1600−800 cm$^{-1}$), is magnified by a factor of 2 to show the small peaks corresponding to the methyl backbone and α-$CH_3$.

**3.1. IRRAS Measurements of PMMA Film Exposed to VUV.** PMMA strongly absorbs ultraviolet radiation[20] at wavelengths less than 160 nm (C−C bonds in the polymer backbone) and near 180 and 210 nm (C−O $\pi$−$\pi^*$ and n-$\pi^*$ transitions in the ester moieties). The high absorption coefficient[26] of PMMA restricts the penetration of the VUV radiation to a very shallow surface layer, around 150 nm thick for 160 nm light. Primary UV photochemical reactions in PMMA are wavelength dependent[13,17,23] and give rise to a variety of chemical reactions such as cross-linking or Norrish reactions[13] as depicted in Figure 1. To quantify the chemical changes caused by VUV light, ≈110 nm thick PMMA films were deposited on Au and exposed to the light from a $D_2$ lamp under vacuum. The chemical changes occurring in the films were identified using IRRAS.

Figure 3 shows the infrared absorption spectra of a ≈110 nm thick PMMA film. The absorption peaks have been assigned previously,[31,32] falling into two groups. The first group consisted of vibrational modes in the ester (−$COOCH_3$) side-chains and the second the vibrational states of the methylene groups in the carbon backbone and the α-$CH_3$ groups. The ester absorption features[32,33] consisted of a single, strong peak at 1740 cm$^{-1}$ (C═O stretch), two sets of double peaks from various ester modes below 1300 cm$^{-1}$ (1270 and 1245 cm$^{-1}$, 1196 and 1153 cm$^{-1}$), the -$OCH_3$ rock mode at 996 cm$^{-1}$ and the ester methyl group C−H stretch ($\nu_{CH}$) modes near 3000 cm$^{-1}$. The second group consisted mostly of $\nu_{CH}$ and H−C−H bending

modes from the backbone and the α-$CH_3$ groups. The α-$CH_3$ bending mode was near 1450 $cm^{-1}$, and the methylene ($-CH_2-$) twisting mode was at 1377 $cm^{-1}$. Several slightly overlapping $\nu_{CH}$ peaks resulted in a multiply peaked feature in the 2800−3000 $cm^{-1}$ region. The sharp peak near 3000 $cm^{-1}$ was from the $\nu_{CH}$ modes in the ester methyl group, and the peak at 2950 $cm^{-1}$ was a superposition of $\nu_{CH}$ modes from backbone $CH_2$ groups, α-$CH_3$ groups and ester $CH_3$ groups. α-$CH_3$ and backbone $CH_2$ groups also contributed to several small peaks on the shoulder of the 2950 $cm^{-1}$ peak, and a well-defined peak near 2850 $cm^{-1}$.[31−33] Comparison of the spectra in Figure 3 to PMMA orientation studies by IRRAS[33] indicated that the repeating units in the polymer film were orientated with the backbones parallel to the surface, and the ester side groups were oriented off the surface normal. The polymer−vacuum interface was largely composed of the PMMA ester groups, as reported in helium atom scattering[34] and sum-frequency generation[35] studies of PMMA thin films.

The changes in the IRRAS spectra caused by exposure of VUV to PMMA clearly show that the primary photochemical mechanism was Norrish type IA (Figure 1, mechanism 3) ester side chain photolysis. As shown in Figure 3, between 1600 and 900 $cm^{-1}$, the absorption features associated with the ester side chain diminished and disappeared altogether with increasing VUV exposure, but absorption features from the backbone carbon chain remained (purple line). As VUV exposure proceeded, the $OCH_3$ stretch mode (1440 $cm^{-1}$) and rocking mode (991 $cm^{-1}$ and 1388 $cm^{-1}$) peaks vanished and the triple peak feature near 1485 $cm^{-1}$ (from α-$CH_3$, -$OCH_3$, and H−C−H bend modes) decreased in intensity and became poorly resolved due to the loss of the ester methyl group. At the center of this feature was a peak at 1450 $cm^{-1}$ that corresponded to the polymer backbone's $-CH_2-$ scissor mode. The intensity of this peak initially decreased but reached a limiting value by 18 000 s (blue line) of VUV exposure. Closer inspection of the $\nu_{CH}$ region between 3150 and 2750 $cm^{-1}$ (Figure 3) highlighted the significance of the ester loss pathway in the modification of PMMA films by VUV radiation. Before irradiation (black line), this portion of the spectrum consisted of two pronounced peaks and a few shoulder peaks, assigned to the symmetric and antisymmetric $\nu_{CH}$ modes from the methylene backbone, the ester $CH_3$, and the α-$CH_3$. The changes in this region clearly indicate the loss of methyl $\nu_{CH}$ and the retention of backbone methylene $\nu_{CH}$, even after very long VUV exposures. As shown by Figure 3, the peak at 2997 $cm^{-1}$ promptly disappeared with a corresponding decrease of the 2950 $cm^{-1}$ peak, due to the loss of the ester methyl groups. It was unclear as to the origin of the small peak at 2843 $cm^{-1}$; one possibility was Fermi resonance between overtones of the bending fundamentals and the $\nu_{CH}$ modes in the methyl substituent. This peak shifted to 2870 $cm^{-1}$ once most of the ester groups had been removed from the film. Significant $\nu_{CH}$ character remained, and further VUV exposure after 5400 s did not significantly change the absorption spectrum; even after 139 080 s (≈38 h), the carbon backbone absorption was not significantly altered.

IRRAS spectra taken after shorter VUV exposures (Figure 4) highlight the evolution of the chemical changes before a significant amount of polymer has been removed. Unlike Figure 3, these spectra used the spectrum of the pre-exposure PMMA film as reference instead of bare Au, in order to highlight the subtle changes at the initial stage of photolysis. The carbonyl absorption features monotonically decreased (negative peaks), as did the C−H stretch peaks assigned to the ester methyl group (2997 and 2950 $cm^{-1}$). Some new IR absorption features emerged during VUV irradiation. New peaks were found at 2975, 2906, 2863, and 1638 $cm^{-1}$, indicating the formation of carbon−carbon double bonds, as observed by previous studies as an intermediary product to polymer cross-linking[36,37] (Figure 4, inset). One study[38] suggested that cross-linking was enhanced when the temperature of polymer was below the glass transition temperature ($T_g$) because of the immobility of polymer strands. In the current experiment, the 1638 $cm^{-1}$ peak rapidly saturated, as would be expected for such an intermediary product. Once the C=C bond was formed, it was subject to rupture by VUV, leaving a C−C single bond, and cross-linked[18,39] polymer backbones.

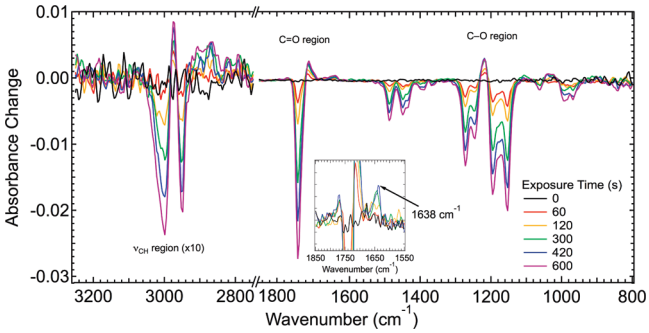


**Figure 4.** IRRAS difference spectra for moderate VUV exposures. The changes in the IRRAS spectra for up to 600 s VUV exposures ($\Phi_{VUV}$ = 350 μW) show the loss of C−H and carbonyl species and the growth of C=C bonds (inset), the first step in cross-linking polymer chains.

It was possible that the changes in $\nu_{CH}$ intensity herein were due to changes in the orientation of the polymer chains relative to the gold substrate, thus modulating the intensity of the absorption features because of the surface dipole selection rule, rather than being the result of chemical changes. However, these experiments were conducted at room temperature, well below the 378 K $T_g$ for PMMA,[40] and the sample temperature did not vary due to VUV exposure, thus the polymer strands should be largely immobile.[41] Furthermore, VUV absorption causes direct photodissociation, rather than conversion of VUV photons to heat in the film,[4] so heating of the film and thermal activation of polymer motion was unlikely, thus the observed changes in the infrared absorption spectra were due to chemical changes rather than disordering of the polymer film.

**3.2. Photochemical Kinetics.** Figure 5A shows the mass loss from PMMA films deposited directly on QCMs as a function of VUV exposure time for four different intensities of VUV radiation. The observed mass loss from the PMMA films (solid lines) showed no initiation period and ceased immediately when the exposures were halted. These data were fit to a single exponential (dashed black lines) given by eq 1, where $m$ was the change in mass measured by the QCM in μg, $m_0$ was the initial mass of the film, $k_{obs}$ was a fitting parameter corresponding to the observed rate constant, and $t$ was the exposure time in seconds.

$$\frac{m}{m_0} = \exp(-k_{obs}t) \quad (1)$$

$$R_{VUV} = FW_{PMMA}\frac{dn_{PMMA}}{dt} = \frac{dm}{dt} = -k_{obs}m \quad (2)$$

The mass loss rate, $R_{VUV}$, followed first order kinetics with respect to the mass of the PMMA film. This was because VUV light penetrates the entire film, rather than just a portion near the


dx.doi.org/10.1021/jp1061368 |J. Phys. Chem. A 2011, 115, 3736–3745

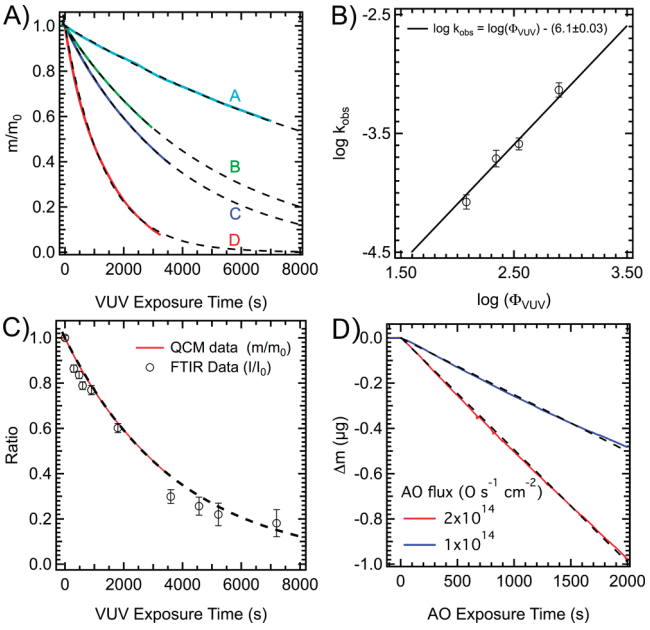


**Figure 5.** QCM measurements of mass changes of PMMA exposed to VUV or AO. Plot (A) shows the mass changes measured with the QCM (colored solid lines) for four different VUV intensities (A − 790 $\mu$W, B − 350 $\mu$W, C − 220 $\mu$W, D − 120 $\mu$W). Exponential fits to each line are shown as dashed black lines. The photoreaction order was determined from the slope of the data shown in (B). The reaction was first order with respect to VUV intensity. The correlation between the QCM measurements (lines) and IRRAS measurements (open black circles) are shown in plot (C). Plot (D) shows the QCM measurements when the PMMA film was exposed to two different fluxes of atomic oxygen. The solid red and blue lines are the experimental data and the dashed black lines are linear fits to the data.

surface. In order to determine the reaction order with respect to VUV flux, the observed rate constant ($k_{obs}$) was plotted against the logarithm of the VUV light intensity, $\Phi_{VUV}$, as shown in Figure 5B. The slope of the linear fit (black line) to the data was found to be unity, therefore the reaction was also first order with respect to $\Phi_{VUV}$. However, because $\Phi_{VUV}$ was constant during each exposure, the observed rates still only depend on the number of absorbers, $n_{PMMA}$. The correlation between the IRRAS and QCM measurements is shown in Figure 5C, where the mass change measured with the QCM (red line), an exponential fit to the QCM data (dashed black line) and the integrated intensity the C═O absorption peak measured with IRRAS (black circles) are plotted. The two data sets agree very well, which indicates that ester photolysis maps onto the observed mass loss.

Upon absorption of a VUV photon a PMMA monomer either dissociates, forming a methyl formate radical, or quenches in some fashion.[42] The quantum yield, $\phi$, is the fraction of photoexcited PMMA monomers that dissociate. The observed rate constant ($k_{obs}$) is the product of the quantum yield, the VUV photon flux ($\Phi_{VUV}$) and the rate constant for VUV absorption ($k_{Abs}$), as shown in eq 3.

$$R_{VUV} = FW_{PMMA}\frac{dn_{PMMA}}{dt} = \frac{dm}{dt} = -k_{obs}m = -\phi\Phi_{VUV}k_{Abs}m_{PMMA} \quad (3)$$

For clarity, $k_{Abs}$ and the quantum yield may be combined into a single constant for VUV irradiation, $k_{VUV}$. The integrated rate law then becomes:

$$\frac{m}{m_0} = \exp(-k_{VUV}\Phi_{VUV}At) \quad (4)$$

Where $A$ was the area of the sample exposed to VUV. The VUV irradiation rate constant, $k_{VUV}$, was calculated to be $(5.4 \pm 0.9) \times 10^9$ W$^{-1}$ (or equivalently $(6.57 \pm 1.18) \times 10^{-19}$ h$\nu^{-1}$). To compare these results to those from others, $\phi$ was calculated from the data in Figure 5A using eq 5. The mass loss rates ($R_{loss}$) for each VUV intensity were approximated with a linear fit to the data between 50 and 550 s.

$$\phi = \frac{\text{No. of dissociated monomers}}{\text{No. of photons absorbed}} = \frac{R_{loss}(N_A/FW_{loss})}{A\Phi_{VUV}(I/I_0)} \quad (5)$$

The IRRAS data and a previous study[29] indicated that the dominant reaction mechanism was Norrish type I methyl formate radical loss, and this radical abstracted a hydrogen from the polymer before being released as methyl formate, so $FW_{loss}$ was 60 g mol$^{-1}$. The ratio, $I/I_0$, was the fraction of photons absorbed by the film, calculated from Beer's Law (eq 6):

$$(I/I_0) = \exp(-2\alpha d) \quad (6)$$

The quantum yield was calculated to be 0.11 ± 0.03, for 110 nm thick films ($d$), and the absorption coefficient, $\alpha$, was $1.2 \times 10^{-5}$ cm$^{-1}$ at 160 nm.[26] Quantum yield varies with the wavelength of the VUV light source, and previous studies have shown that the quantum yield is 0.053 at 185 nm,[43] 0.03 at 215−230 nm,[44] and ~0.92 at 254 nm.[16]

Previous mass spectrometric studies of 200−300 nm UV irradiation of PMMA films from this group[29] and others[2] showed the major products were methyl formate formed by mechanism 3 in Figure 1. The VUV-induced photochemical changes measured with IRRAS showed that although main chain scission is energetically accessible, ester side group cleavage was still the major photochemical process, despite the higher energy radiation. This was supported by studies of other polymeric materials[6,45] and demonstrates that even though the reagents have sufficient energy to access several different reaction channels, the rate of ester cleavage in the ultraviolet photodissociation of thin PMMA films was much greater than the other possible reaction mechanisms. The main photochemical reaction pathway did not vary with the wavelength of the UV light source, but reaction rate changed, resulting in a wavelength dependence of quantum yield.

**3.3. Surface Morphological Changes.** The IRRAS and QCM data clearly show that for short and intermediate exposures, the PMMA films were drastically changed. After long exposures to VUV, the PMMA film was extensively modified and only a carbonaceous residue remained. AFM was employed to measure the effect of VUV exposure on the surface morphology. AFM is a powerful tool for the measurement of surface structure; previous work from our group demonstrated the ability of the same AFM system to measure defect healing in thin polymer films[46] and the morphological changes dues to VUV irradiation of Au, Ag, and Cr films on PMMA.[47] A previous AFM study[48] of VUV-irradiated PMMA showed an initial smoothing of the PMMA surface due to higher reactivity of surface defects. An AO/VUV ablation study[30] of PVDF polymers used scanning electron microscopy (SEM) to show

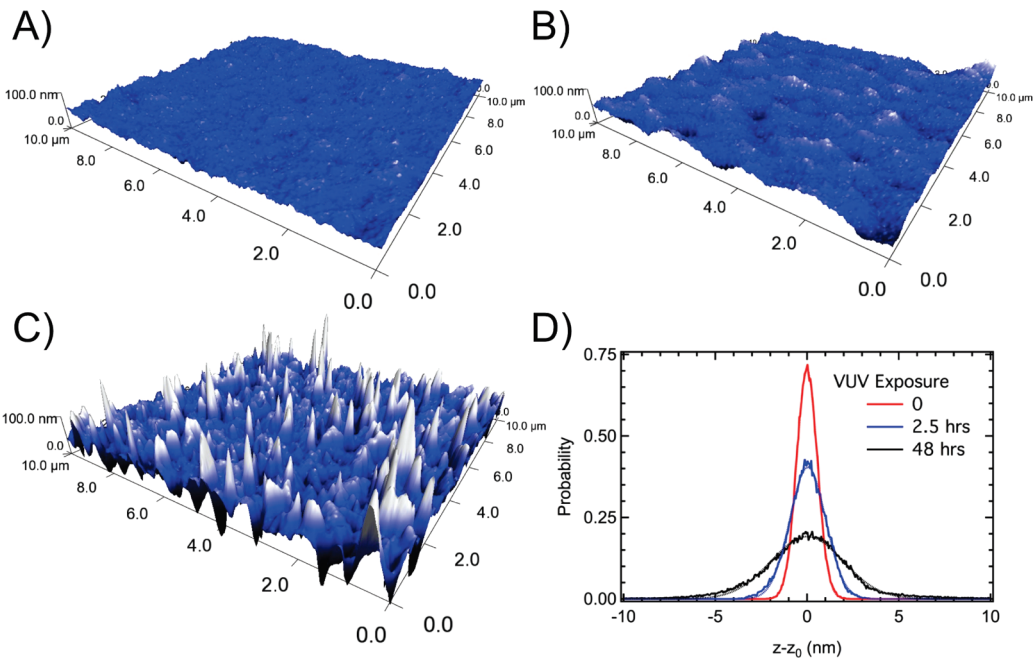


**Figure 6.** AFM images of VUV-irradiated films. (A) Before irradiation, (B) after 2.5 h of VUV exposure, (C) after 48 h of VUV exposure, and (D) distribution of the pixel heights for each image. The vertical scale of the images is 100 nm to highlight increased roughness of the PMMA film. AFM conditions are provided in the text.

**Table 1. AFM Data**

| VUV exposure time (h) | $R_q$ (nm) | $R_a$ (nm) | thickness (nm) | refractive index ($n$) |
|---|---|---|---|---|
| 0 | 0.809 | 0.642 | $120 \pm 10$ | 1.4893 |
| 2.5 | 1.35 | 1.05 | $116 \pm 8$ | 1.4895 |
| 48 | 2.71 | 1.96 | $56 \pm 12$ | 1.5010 |

that at short exposure times, the surface remained smooth, but as the film thinned, it became more pitted.

The surface morphology and the thickness of the PMMA film after VUV exposure were measured with AFM and ellipsometry. AFM images of a 110 nm thick PMMA film on Au were taken before exposure (Figure 6A), after 2.5 h (Figure 6B), and after 48 h (Figure 6C) of continuous VUV irradiation. Table 1 lists the topological data from these images as well as the thickness data from ellipsometry measurements. Two parameters, the arithmetic roughness ($R_a$) and the root-mean square roughness ($R_q$), were used to quantify the roughness of the polymer surface.[49] $R_a$ and $R_q$ were calculated using eqs 7 and 8, where $z_i$ was the height at pixel $i$, $n$ was the number of pixels in the image (each image was 256 by 256 pixels), and $z_0$ was the mean surface level, given by eq 9.

$$R_a = \frac{1}{n}\sum_{i=1}^{n} |z_i - z_0| \tag{7}$$

$$R_q = \sqrt{\frac{1}{n}\sum_{i=1}^{n} (z_i - z_0)^2} \tag{8}$$

$$z_0 = \frac{1}{n}\sum_{i=1}^{n} z_i \tag{9}$$

Also shown with the AFM images is the distribution of the heights of each pixel (Figure 6D). These show a normal distribution of pixel heights for all VUV exposures with the width ($R_q$) increasing with exposure time. Before exposure (Figure 6A), the PMMA film surface was smooth with only a few small pits and bumps. After 2.5 h of VUV exposure ($I$ = 120 $\mu$W cm$^{-2}$) (Figure 6B), there was a slight increase in the corrugation, as evidenced by $R_q$ increasing by only 50% to 1.35 nm, but the morphology of the PMMA film surface was not significantly altered. Ellipsometry measurements showed about a 5 nm decrease in the thickness of the film, which was in reasonable agreement with the QCM mass loss measurements; using the mass loss measured by the QCM and assuming the density of the film was unchanged, the same 2.5 h exposure would corresponded to about a 10 nm decrease in film thickness. After these shorter exposures, the resultant film showed a roughness similar to a previous study,[48] where $R_q$ was reported to be 2 nm or less after 3000 s of VUV exposure of equivalent intensity. After prolonged (48 h) VUV exposure, however, the resultant film was significantly rougher and pitted (Figure 6C), with many bumps that are 10−20 nm high and up to 500 nm in diameter, resulting in $R_q$ (the width of the height distribution) increasing more than 3-fold to 2.71 nm. A similar morphological change was observed on UV-irradiated PVDF.[50,51] In the current study, the film was reduced to about half its initial thickness (56 nm), and the refractive index changed as well, increasing from 1.4893 to 1.501, which is characteristic of C=C bond formation and C−C cross-linking in the film.[50,51]

The chemical and physical changes to the film did not necessarily take place at the same time, as inspection of the QCM/IRRAS and AFM/ellipsometry results have shown. The most dramatic chemical changes occurred within the first hour of exposure, where the film thickness and morphology were not drastically altered. As exposure continued, no new IR absorption peaks were observed,


dx.doi.org/10.1021/jp1061368 |J. Phys. Chem. A 2011, 115, 3736–3745

and the steady loss of ester side chains resulted in a thinner film, as shown by the ellipsometry data in Table 1. After prolonged exposure, the chemical nature of the remaining film was difficult to discern, but it was clearly no longer PMMA (Figure 3). Almost all the carbonyl absorption features disappeared, and the remaining absorption features were from $\nu_{CH}$ modes, so the film likely became a branched hydrocarbon film due to photon-induced volatilization of oxygen-containing functional groups and cross-linking of the polymer backbones. The film was reduced to about half its initial thickness, and its surface became very rough. One possible cause for the increased roughness of the film was phase separation between the unaltered PMMA and the photolyzed material.[52] Another possibility was that because the films were at room temperature during the exposure, the mobility of both the original PMMA and the solid photolysis products would be low[40,41,53] and could not diffuse to fill in any pits formed.[46,56] Tabulated $T_g$ values for branched hydrocarbon polymers were 337 K for poly(*tert*-butylethylene) and 326 K for poly-(3,3-dimethylbutylethylene),[54] indicating that although $T_g$ may decrease, the $T_g$ for the residual film was still likely to be greater than room temperature. Furthermore, the formation of the thicker cross-linked chains may result in ridges that run through the film, appearing as high spots in the AFM images.

**3.4. Atomic Oxygen (AO) and VUV/AO Reactions with PMMA.** The change in the mass of PMMA thin films exposed to gas-phase oxygen atoms ($O(^3P)$, $E_{trans}$ = 25 kJ mol$^{-1}$) were measured. In addition, PMMA films deposited on the QCM were exposed sequentially to AO, VUV, as well as to both simultaneously, to investigate the existence of any synergistic effect between VUV and AO. In the range of fluxes we used in this paper, when the mass loss rates caused by individual exposure were comparable, the mass loss rate due to simultaneous exposure to both reagents was found to be less than the sum of the two processes alone. A similar study of the erosion of FEP and PMMA[2] reported that the ablation rate was not enhanced by coexposure of AO and VUV, but it used much higher energy ($E_{trans}$ = 520 kJ mol$^{-1}$) oxygen atoms and an identical VUV source and determined that hyperthermal AO causes much more mass loss than VUV or hyperthermal Ar bombardment. Our study differs in two important ways. First, the prior experiments used thick polymer samples, so it was possible that bulk processes overwhelmed any difference in the kinetics of the near-surface region investigated here. Second, although the average fluxes of atomic oxygen were about the same, the higher energy experiments employed a pulsed AO source where the individual pulses were about 2 orders of magnitude more intense than for the continuous source used here. In both cases, the incident flux of atomic oxygen ($\approx 10^{14}$ O atoms/cm$^2$) was less than the surface atom density ($\approx 10^{15}$ atoms/cm$^2$).

Figure 5D shows the mass change of a 110 nm thick PMMA film when exposed to gas-phase atomic oxygen for two different fluxes of atomic oxygen, $2 \times 10^{14}$ O atoms s$^{-1}$ cm$^{-2}$ (red line) and $1 \times 10^{14}$ O atoms s$^{-1}$ cm$^{-2}$ (blue line). The mass loss rate due to atomic oxygen was similar in magnitude as VUV and no induction period was observed. However, rather than the first-order kinetics observed with VUV, the mass loss was zeroth order with respect to the PMMA film thickness, consistent with reaction at the surface. The kinetic model was set up in eq 10:

$$R_{AO} = \frac{dm_{PMMA}}{dt} = -k_{obs} \quad (10)$$

The integrated rate law is simply:

$$\Delta m_{PMMA} = -k_{obs}\Delta t \quad (11)$$

Because doubling the flux of oxygen atoms doubled the rate (given by the slopes in Figure 5D, dashed black lines), the reaction was first order with respect to incident atomic oxygen flux. The observed rate constant, $k_{obs}$, was the product of the incident flux ($\Phi_{AO}$), the area of the atomic oxygen beam ($A_{AO}$) on sample, and the actual rate constant for reaction between oxygen atoms and PMMA ($k_{AO}$), so eq 11 becomes:

$$\Delta m_{PMMA} = -k_{AO}A_{AO}\Phi_{AO}\Delta t \quad (12)$$

The value of $k_{AO}$ was found to be $(8.82 \pm 0.26) \times 10^{-18}$ $\mu$g per O atom. These results indicate that at initial stage of oxidation, the reaction occurred exclusively at the vacuum–polymer interface, the density of reaction sites on the polymer surface remained nearly constant and significantly larger than the incident oxygen flux, thus the incident oxygen atoms were the limiting reagent.

The apparent zeroth order kinetics were the result of the incident oxygen atoms having sufficient kinetic energy to abstract hydrogen from PMMA. Based on electronic structure calculations[13] and crossed-beam studies of the reactions of atomic oxygen atoms with small alkanes,[55−58] hydrogen abstraction was the major process of low energy (<200 kJ mol$^{-1}$) $O(^3P)$ oxidation of hydrocarbons. Mass loss from PMMA by atomic oxygen was activated by $E_{trans}$, but the kinetics were non-exponetial.[2] Crossed-beam studies[55−58] showed that the activation energy for abstraction of primary H was 29 kJ mol$^{-1}$, secondary H was 19 kJ mol$^{-1}$, and tertiary H was 14 kJ mol$^{-1}$. In the PMMA repeating unit, there are both primary and secondary hydrogens (Figure 1). The $E_{trans}$ of the incident O atoms (25 kJ mol$^{-1}$) was slightly below the threshold energy for abstraction of primary hydrogens, thus it would be expected that the reactivity should be dominated by abstraction of secondary hydrogens from the polymer backbone. The propagated reactions followed the schemes suggested by Lianos, et al.,[59] where radicals were formed on polymer chains after hydrogen abstraction and further reacted with $O(^3P)$ yielding alkoxyradicals, or in some cases with $O_2$ to form peroxyradicals, which lead to reactions by hydrogen transfer or reorganization.[56] These reactions lead to polymer chain scission and mass loss through the production of small volatile molecules.

The erosion due to the beam was quantified by the erosion yield ($Y_E$) given by eq 13.[30] The erosion yield was the ratio of the mass loss ($\Delta$m, $\mu$g s$^{-1}$) and the product of the density of the polymer film ($\rho$, 1.17 $\times$ 10$^6$ $\mu$g cm$^{-3}$), the incident beam flux ($\Phi_{AO}$, 2.0 $\times$ 10$^{14}$ O atoms s$^{-1}$ cm$^{-2}$), and the area of the beam at the sample ($A$, 0.28 cm$^2$). This term allowed for comparison of results from measurements taken under a variety of different conditions.

$$Y_E = \frac{\Delta m}{A\rho\Phi_{AO}} \quad (13)$$

From the data in Figure 5D, the erosion yield of PMMA by the AO beam was calculated to be $4.20 \times 10^{-23}$ cm$^3$ per oxygen atom. This was greater than the yield reported for AO erosion of PVDF,[30] which was $2.8 \times 10^{-24}$ cm$^3$ per oxygen atom. This difference was likely due to a combination of the inherently greater reactivity of PMMA toward atomic oxygen and the nature of the atomic oxygen source. The PVDF experiments were

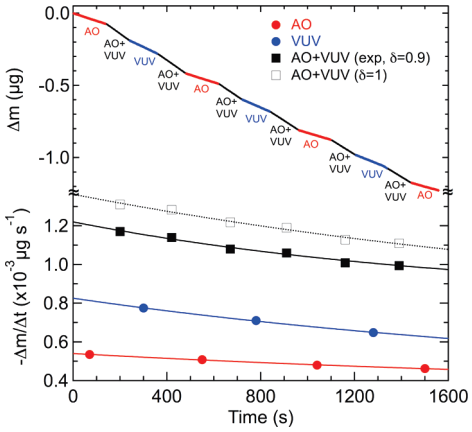


**Figure 7.** QCM measurement during sequential exposures of atomic oxygen and VUV. A 110 nm thick PMMA film was deposited directly on the QCM and was sequentially exposed to oxygen atoms (red), VUV (blue), and both simultaneously (black). The top portion shows the QCM data directly and the lower plots the rate of mass loss during each exposure type. The open black squares (□) are the direct sums of the rates from exposure to either AO or VUV alone, where $\delta = 1$. The experimental data (■) yield $\delta = 0.9$. Conditions are given in the text.

performed with a low energy plasma source with the $E_{trans}$ of oxygen atoms only about 4 kJ mol$^{-1}$, whereas the experiments here used a supersonic beam of O atoms with a higher average $E_{trans}$ of 25 kJ mol$^{-1}$, opening more reaction pathways on PMMA.

The significance of any synergistic effects when polymeric materials were exposed to both UV/VUV and oxygen atoms has been debated and seems to be highly dependent on the polymer and the relative energies and fluxes of the reagents.[12] It is essential that the relative reactivity from either AO or VUV be properly balanced to study this effect. If the reactivity from one reagent overwhelms the contribution from the other, any cooperative effect would be obscured. A synergistic effect is the observation of a reaction rate for the combined exposure different from the sum of the rates measured during the individual, separate exposures. Experimental studies of atomic oxygen and UV erosion for several polymeric systems showed varying results, in some cases the combination enhanced reaction due to additional bond breaking,[1,7,8,22,60] but in others either had little effect or even decreased the erosion rate by increasing cross-linking of polymer strands,[9−11,61] and theoretical models were also inconclusive on this phenomenon.[4,13] Previous studies have found that a synergistic acceleration of polymide mass loss occurred when the relative atomic oxygen flux is low against VUV flux.[23,25] In the present study, the relative flux of VUV and atomic oxygen were controlled by varying the distance between the sample and the VUV light source and/or reducing the AO flux from the oxygen beam.

The mass changes for 110 nm thick PMMA films were measured with the QCM during exposure to AO, VUV, and both AO and VUV. The top portion of Figure 7 shows the measured mass changes during sequential exposure to atomic oxygen (red), VUV (blue), and both at the same time (black). Varying the order of exposure neither altered the observed mass loss nor the overall trends, since the VUV and atomic oxygen fluxes were low, and the sample was still considered as relatively pristine after these exposures. The lower portion of Figure 7 shows the average rate of mass change for each exposure type: atomic oxygen reaction (closed red circles), VUV (closed blue circles), simultaneous exposure to both VUV and AO (closed black squares), and the direct sum of the individual reaction rates for exposure to AO and VUV only (open black squares). The previously determined values of $k_{VUV}$ and $k_{AO}$ were used to generate the fit lines shown in the figure for each exposure type. As shown, simultaneous exposure of the two reagents did not result in an enhancement of the mass loss rate. Instead, the reaction rate was lower than the direct sum of the reaction rates from exposure to each reagent individually, which suggests that the two reactive processes interfered with each other. A possible cause for the hindered mass loss in the presence of both oxygen atoms and VUV was that if VUV photolysis were rapid, there would be fewer sites for incident oxygen atoms to abstract hydrogen, effectively shutting off this reactive channel. Instead of causing mass loss, oxygen atoms may have added to the photochemical radicals or the remaining polymer. VUV photons would then cleave these oxidized functionalities in similar ways to the photolysis of hydroperoxides in polymers.[62] As a result, oxidation combined with UV photolysis reduces the rate of mass loss from direct VUV photolysis of the PMMA repeating unit or volatile molecules produced by oxidation.

To quantify the effect of simultaneous exposure on the rate of mass loss ($R_{loss}$), the synergistic efficacy, $\delta$, was determined as given in eq 14:

$$R_{loss} = \frac{dm}{dt} = \delta(R_{AO} + R_{VUV}) \qquad (14)$$

The value of $\delta$ indicates how AO and VUV act in conjunction. If $\delta$ were unity, then there would be no synergistic effect, for the combined reaction rate would be purely additive. For values of $\delta > 1$ there is positive synergistic effect between the two reagents, and for values of $\delta < 1$ there is a negative synergistic effect. To determine $\delta$, the expected mass losses for each exposure interval in Figure 7 were calculated. For a particular time interval, $\Delta t$, the mass loss was:

$$\Delta m_{QCM} = \delta(-k_{AO}A_{AO}\Phi_{AO}\Delta t - m_i[\exp(-k_{VUV}A\Phi_{VUV}\Delta t)]) \qquad (15)$$

where $m_i$ was the mass of the film at the start of the exposure, and $\Delta m_{QCM}$ was the mass loss measured with the QCM in interval $\Delta t$. The calculated reaction rates if $\delta = 1$ are plotted in Figure 7 as open squares and a dotted line. The reaction rates measured during coexposure are plotted as closed squares in Figure 7, and comparison of the two data sets clearly show that $\delta$ was less than unity. The average value for the five simultaneous intervals was found to be 0.9, indicating the existence of an inhibitory synergistic effect between VUV and atomic oxygen reactions on PMMA.

## 4. CONCLUSION

The kinetics of the reactions between thin films of PMMA and VUV and AO were measured with in situ IRRAS, in situ QCM, ex situ AFM, and ellipsometry. These measurements clearly demonstrated the capability to detect chemical changes within the polymer film in real time. The combination of these methods enabled the determination of the mechanisms of different reactions.

The primary photochemical reaction was ester side chain photolysis, which followed first order kinetics with respect to PMMA film thickness. AFM measurements of the PMMA surface morphology showed that VUV exposure roughened the film.

The relative intensities of VUV light and atomic oxygen were carefully tuned to be on a similar level to study the significance of synergistic effects under such conditions. Although the rate of mass loss during simultaneous VUV/oxygen exposure was greater than either VUV or atomic oxygen alone, it was less than the sum of the individual rates, indicating that at these relative fluxes, a negative synergy exists among the reagents. The kinetics of the two modification processes indicated the nature of the reactions. Because VUV light penetrated the entire film, the light interacted with all the molecules in the film, and the resulting photochemistry followed first-order kinetics with respect to film thickness. For thick PMMA samples, the light would only penetrate into the near-surface region, and the observed kinetics would not depend on film thickness. Likewise, for atomic oxygen, the observation of zeroth-order kinetics with respect to film thickness was the result of the reaction between AO and PMMA being exclusively a surface process.

In this paper, we explored the reactivity of atomic oxygen and VUV light and their combined effects on PMMA thin film. In the regime of the relative flux of this study, we observed a synergy leading to a decrease in the mass loss rate of PMMA. Understanding the kinetics and dynamics of the reaction chemistry of this polymer system is not only fundamental to photochemistry and surface oxidation, but is also important for technical issues such as plasma processing and the design of spacecraft materials.

## AUTHOR INFORMATION


### Corresponding Author

*E-mail: s-sibener@uchicago.edu.

### Present Addresses

[†]Center for Nanomaterials, Argonne National Laboratory, 9700 S. Cass Ave., Argonne, IL 60439.

[‡]Sloan Annex, MC-114-36, California Institute of Technology, Pasadena, CA 91126.


## ACKNOWLEDGMENT

We would like to thank Kevin Gibson and James Becker for helpful discussions. This work was supported by the Air Force Office of Scientific Research and through the NSF-Materials Research Science and Engineering Center at The University of Chicago, NSF-DMR-0213745.

## REFERENCES


(1) Grossman, E.; Gouzman, I. *Nucl. Instrum. Methods Phys. Res., Sect. B* **2003**, *208*, 48.

(2) Zhang, J.; Lindholm, N. F.; Brunsvold, A. L.; Upadhyaya, H. P.; Minton, T. K.; Tagawa, M. *ACS Appl. Mater. Interfaces* **2009**, *1*, 653.

(3) Kleiman, J. I.; Iskanderova, Z. A.; Perez, F. J.; Tennyson, R. C. *Surface Coat. Technol.* **1995**, *77*, 827.

(4) Conforti, P. F.; Prasad, M.; Garrison, B. J. *Acc. Chem. Res.* **2008**, *41*, 915.

(5) Kleiman, J. I.; Gudimenko, Y. I.; Iskanderova, Z. A.; Tennyson, R. C.; Morison, W. D.; McIntyre, M. S.; Davidson, R. *Surf. Interface Anal.* **1995**, *23*, 335.

(6) Brunsvold, A. L.; Zhang, J. M.; Upadhyaya, H. P.; Minton, T. K. *ACS Appl. Mater. Interfaces* **2009**, *1*, 187.

(7) Moreau, W. M. *Semiconductor Lithography: Principles, Practices, and Materials*; Plenum Press: New York, 1988.

(8) Lippert, T. *Plasma Processes Polym.* **2005**, *2*, 525.

(9) Normand, F.; Marec, J.; Leprince, P.; Granier, A. *Mater. Sci. Eng., A* **1991**, *139*, 103.

(10) Murakami, T. N.; Fukushima, Y.; Hirano, Y.; Tokuoka, Y.; Takahashi, M.; Kawashima, N. *Colloids Surf., B* **2003**, *29*, 171.

(11) Skurat, V. *Nucl. Instrum. Methods Phys. Res., Sect. B* **2003**, *208*, 27.

(12) Yokota, K.; Ohmae, N.; Tagawa, M. *Space Technol. Proc.* **2006**, *6*, 141.

(13) Conforti, P. F.; Garrison, B. J. *Chem. Phys. Lett.* **2005**, *406*, 294.

(14) Prasad, M.; Conforti, P. F.; Garrison, B. J. *Appl. Phys. A: Mater. Sci. Process.* **2008**, *92*, 877.

(15) Srinivasan, R.; Braren, B.; Seeger, D. E.; Dreyfus, R. W. *Macromolecules* **1986**, *19*, 916.

(16) Gupta, A.; Liang, R.; Tsay, F. D.; Moacanin, J. *Macromolecules* **1980**, *13*, 1696.

(17) Mitsuoka, T.; Torikai, A.; Fueki, K. *J. Appl. Polym. Sci.* **1993**, *47*, 1027.

(18) Wochnowski, C.; Metev, S.; Sepold, G. *Appl. Surf. Sci.* **2000**, *154*, 706.

(19) Kuper, S.; Modaressi, S.; Stuke, M. *J. Phys. Chem.* **1990**, *94*, 7514.

(20) Fozza, A. C.; Roch, J.; KlembergSapieha, J. E.; Kruse, A.; Hollander, A.; Wertheimer, M. R. *Nucl. Instrum. Methods Phys. Res., Sect. B* **1997**, *131*, 205.

(21) Tagawa, M.; Yokota, K.; Ohmae, N. *J. Spacecr. Rockets* **2004**, *41*, 345.

(22) Rasoul, F. A.; Hill, D. J. T.; George, G. A.; O'Donnell, J. H. *Polym. Adv. Technol.* **1998**, *9*, 24.

(23) Tagawa, M.; Yokota, K. *Acta Astronaut.* **2008**, *62*, 203.

(24) Gugumus, F. *Polym. Degrad. Stab.* **2002**, *75*, 309.

(25) Riedel, D.; Castex, M. C. *Appl. Phys. A: Mater. Sci. Process.* **1999**, *69*, 375.

(26) Kudo, K.; Miyazaki, K.; Sakai, H.; Iwabuchi, T.; Mutoh, K.; Miyata, T.; Tomiki, T. *Jpn. J. Appl. Phys., 1* **1992**, *31*, 401.

(27) Sibener, S. J.; Buss, R. J.; Ng, C. Y.; Lee, Y. T. *Rev. Sci. Instrum.* **1980**, *51*, 167.

(28) Zion, B. D.; Sibener, S. J. *J. Phys. Chem. C* **2008**, *112*, 5961.

(29) Cisse, A. L.; Grossman, E.; Sibener, S. I. *J. Phys. Chem. B* **2008**, *112*, 7166.

(30) Dargaville, T. R.; Celina, M.; Martin, J. W.; Banks, B. A. *J. Polym. Sci., B* **2005**, *43*, 2503.

(31) Lipschitz, I. *Polym.-Plast. Technol. Eng.* **1982**, *19*, 53.

(32) Brinkhuis, R. H. G.; Schouten, A. J. *Macromolecules* **1991**, *24*, 1496.

(33) Dybal, J.; Krimm, S. *Macromolecules* **1990**, *23*, 1301.

(34) Freedman, M. A.; Rosenbaum, A. W.; Sibener, S. J. *Phys. Rev. B* **2007**, *75*, 4.

(35) Wang, J.; Chen, C. Y.; Buck, S. M.; Chen, Z. *J. Phys. Chem. B* **2001**, *105*, 12118.

(36) Truica-Marasescu, F. E.; Wertheimer, M. R. *Macromol. Chem. Phys.* **2005**, *206*, 744.

(37) Mikheev, Y. A.; Ershov, Y. A. *Russ. J. Phys. Chem.* **2004**, *78*, 661.

(38) Dickens, B.; Martin, J. W.; Waksman, D. *Polymer* **1984**, *25*, 706.

(39) Choi, J. O.; Moore, J. A.; Corelli, J. C.; Silverman, J. P.; Bakhru, H. *J. Vac. Sci. Technol. B* **1988**, *6*, 2286.

(40) Freedman, M. A.; Becker, J. S.; Rosenbaum, A. W.; Sibener, S. J. *J. Chem. Phys.* **2008**, *129*, 9.

(41) Kim, S. S.; Tsay, F. D.; Gupta, A. *J. Phys. Chem.* **1987**, *91*, 4851.

(42) Berry, R. S.; Rice, S. A.; Ross, J. *Physical Chemistry*: 2nd ed.; Oxford University Press: New York, 2000.

(43) Srinivasan, R.; Lazare, S. *Polymer* **1985**, *26*, 1297.

(44) Schultz, A. R.; Frank, P.; Griffing, B. F.; Young, A. L. *J. Polym. Sci., B* **1985**, *23*, 1749.

(45) Troya, D.; Schatz, G. C. *Int. Rev. Phys. Chem.* **2004**, *23*, 341.

(46) Yufa, N. A.; Li, J.; Sibener, S. J. *Polymer* **2009**, *50*, 2630.

(47) Yufa, N.; Fronk, S.; Darling, S. B.; Divan, R.; Lopes, W.; Sibener, S. J. *Soft Matter* **2009**, *5*, 1683.

(48) Hozumi, A.; Masuda, T.; Hayashi, K.; Sugimura, H.; Takai, O.; Kameyama, T. *Langmuir* **2002**, *18*, 9022.

(49) El Feninat, F.; Elouatik, S.; Ellis, T. H.; Sacher, E.; Stangel, I. *Appl. Surf. Sci.* **2001**, *183*, 205.

(50) Baker, A. K.; Dyer, P. E. *Appl. Phys. A: Mater. Sci. Process.* **1993**, *57*, 543.
(51) Fozza, A. C.; Klemberg-Sapieha, J. E.; Wertheimer, M. R. *Plasmas Polym.* **1999**, *4*.
(52) Kaczmarek, H.; Chaberska, H. *Appl. Surf. Sci.* **2009**, *255*, 6729.
(53) Prucker, O.; Christian, S.; Bock, H.; Ruhe, J.; Frank, C. W.; Knoll, W. *Macromol. Chem. Phys.* **1998**, *199*, 1435.
(54) *Polymer Handbook*: 4th ed.; John Wiley & Sons, Inc.: Hoboken, NJ, 1999; Vol. 1.
(55) Kleinermanns, K.; Luntz, A. C. *J. Chem. Phys.* **1982**, *77*, 3533.
(56) Kleinermanns, K.; Luntz, A. C. *J. Chem. Phys.* **1982**, *77*, 3774.
(57) Andresen, P.; Luntz, A. C. *J. Chem. Phys.* **1980**, *72*, 5842.
(58) Luntz, A. C.; Andresen, P. *J. Chem. Phys.* **1980**, *72*, 5851.
(59) Lianos, L.; Parrat, D.; Hoc, T. Q.; Duc, T. M. *J. Vac. Sci. Technol. A* **1994**, *12*, 2491.
(60) Stiegman, A. E.; Brinza, D. E.; Laue, E. G.; Anderson, M. S.; Liang, R. H. *J. Spacecr. Rockets* **1992**, *29*, 150.
(61) Skurat, V. E.; Samsonov, P. V.; Nikiforov, A. P. *High Perform. Polym.* **2004**, *16*, 339.
(62) Gugumus, F. *Polym. Degrad. Stab.* **1990**, *27*, 19.